Available online at www.sciencedirect.com
ScienceDirect
Journal of Power Sources 160 (2006) 698–703
JOURNAL OF POWER SOURCES
www.elsevier.com/locate/jpowsour

The preparation of $NaV_{1-x}Cr_xPO_4F$ cathode materials for sodium-ion battery

Haitao Zhuo [a], Xianyou Wang [a,*], Anping Tang [a], Zhiming Liu [a], Sergio Gamboa [b], P.J. Sebastian [b]

[a] *College of Chemistry, Xiangtan University, Hunan 411105, China*
[b] *Solar-Hydrogen-Fuel Cell Group, CIE-UNAM, Temixco 62580, Morelos, Mexico*

Received 1 December 2005; received in revised form 18 December 2005; accepted 22 December 2005
Available online 14 February 2006

Abstract

The key to development of sodium-ion battery is the preparation of cathode/anode materials. Cr doped $NaV_{1-x}Cr_xPO_4F$ ($x = 0$, 0.04, 0.08) were prepared by the high temperature solid-state reaction for the application of cathode material of sodium-ion batteries. The structures and morphologies of the cathode materials were characterized by Flourier-infrared spectra (FT-IR), X-ray diffraction (XRD) and scanning electron microscope (SEM). The effects of Cr doping on performances of the cathode materials were analyzed in terms of the crystal structure, charge–discharge curves and cycle performances. The results showed that the as-prepared Cr-doped materials have a better cycle stability than the un-doped one, an initial reversible capacity of 83.3 mAh g^{-1} can be obtained, and the first charge–discharge efficiency is about 90.3%. In addition, it was also observed that the reversible capacity retention of the material is still 91.4% in the 20th cycles.

Keywords: Sodium ion battery; Cathode materials; Capacity; Capacity retention; Cr doping; $NaV_{1-x}Cr_xPO_4F$

1. Introduction

Lithium rechargeable batteries are now well established as power sources for portable electronic equipments such as cellular phone, camcorder and laptop computer. If rechargeable sodium-ion batteries with good performance characteristics could be developed, it would have some significant advantages over lithium-ion batteries, notably a reduction in raw materials cost and the ability to utilize electrolyte systems of lower decomposition potential (due to the higher half-reaction potential for sodium relative to lithium) [1]. So, sodium-ion batteries will be a kind of promising novel batteries.

With the development of anode materials in sodium-ion batteries [1–7], the studies of cathode materials with high performances will become more and more important. Recently, a number of studies about cathode materials have been reported [8,9], for example, Na_xCoO_2, Na_xMnO_2 [8], Na_xTiS_2, $Na_xNbS_2Cl_2$, Na_xWO_{3-x}, $Na_xV_{0.5}Cr_{0.5}S$, Na_xMoS_3, Na_xTaS_2 [9–13] and so on. However, the bad reversibility of intercalation and deintercalation of sodium-ion in above materials and the lower reversible capacity or the greater transferring resistance of the materials have limited their commercial use.

Recently, Barker et al. reported that the $NaVPO_4F$ was used in conjunction with commercially available hard carbon material to form viable sodium-ion batteries [14–17]. The average discharge voltage for the sodium-ion battery was determined to be about 3.7 V, a figure comparable with commercially available lithium-ion cells. But the discharge capacity of $NaVPO_4F$ was declined to less than by 50% of its initial discharge capacity after 30 charge/discharge cycles. Although $NaVPO_4F$ is currently considered one of the most hopeful cathode materials for sodium-ion battery, its performance should be highly improved by modification or doping technology. It is well known that doping technology has been widely used in lithium-ion battery to improve the capacity retention [18,19]. In this paper, $NaVPO_4F$ were synthesized with a high temperature solid-state reaction, and Cr was doped into this material to prepare $NaV_{1-x}Cr_xPO_4F$ ($x = 0$–0.1) powders. The effects of Cr doping on structure and

* Corresponding author. Tel.: +86 732 8293371; fax: +86 732 8292061.
E-mail address: wxianyou@yahoo.com (X. Wang).

0378-7753/$ – see front matter © 2006 Elsevier B.V. All rights reserved.
doi:10.1016/j.jpowsour.2005.12.079

electrochemical properties of $NaV_{1-x}Cr_xPO_4F$ are discussed based on FT-IR, XRD, SEM, charge–discharge curves and cycle performances.

2. Experimental

2.1. Preparation of $NaV_{1-x}Cr_xPO_4F$

The $NaV_{1-x}Cr_xPO_4F$ samples used in this study were all prepared using a carbothermal reduction (CTR) method [16,17] using VPO_4 as a reaction intermediate. The precise CTR reaction conditions for the VPO_4 preparation were determined by a semi-empirical approach based on the thermodynamic requirements for a V^{5+} to V^{3+} transition. The reaction mechanism of VPO_4 preparation may be summarized as fellow:

$$0.5V_2O_5 + NH_4H_2PO_4 + C \rightarrow VPO_4 + NH_3 + 1.5H_2O + CO \quad (1)$$

The precursors, V_2O_5, $NH_4H_2PO_4$, and carbon were intimately mixed and then pelletized. To enable complete vanadium reduction and to ensure the presence of residual carbon in the product phase, a 20% mass excess of carbon was used over the stoichiometric conditions based on reaction (1). The precursor mixture was heated to an ultimate reaction temperature of 750 °C and held for 4 h inside a temperature-controlled tube furnace.

Thereafter, the stoichiometric amounts of Cr_2O_3 and $(NH_4)_2HPO_4$ were mixed using ball mill and the powder was pressed into pellets. The pellets were initially heated to 500 °C for 6 h, and then reground. Pellets were remade and subsequently calcined at 1050 °C for 6 h.

In the second stage of preparation, the VPO_4 and $CrPO_4$ were further reacted with the alkali fluoride to yield the single-phase products $NaV_{1-x}Cr_xPO_4F$

$$NaF + (1-x)VPO_4 + xCrPO_4 \rightarrow NaV_{1-x}Cr_xPO_4F \quad (2)$$

2.2. Materials characterization

(1) Infrared spectra were recorded on Fourier transform infrared (FTIR) spectrometer (Perkin-Elmer Spectrum one) in the wavelength range from 4000 to 500 cm^{-1}, using the KBr disk method.

(2) X-ray diffraction (XRD) of $NaV_{1-x}Cr_xPO_4F$ was performed on a diffractometer (D/MAX-3C) with Cu Kα radiation and a graphite monochromator at 50 kV, 100 mA.

(3) Scanning electron microscopy (SEM), modified 5000 times with 20 kV voltage, was also employed to characterize the prepared powders.

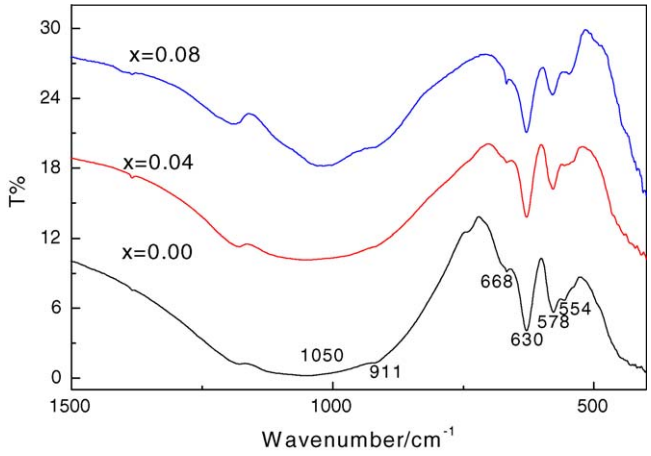

Fig. 1. FT-IR spectra of $NaV_{1-x}Cr_xPO_4F$.

2.3. Electrochemical measurement

The cathode was prepared by mixing the active material with carbon black and PTFE in a weight ratio of 75:15:10. The mixture was pressed onto stainless steel mesh used as current collector and dried under vacuum at 120 °C for 24 h. The simulated battery consisting of the cathode, the sodium foils as an anode and 1 $MNaClO_4$–EC/DMC (1:1 in volume) as an electrolyte were assembled in an argon-filled glove box. Charge/discharge tests were performed between 3.0 and 4.5 V at a rate of 0.1 C at 30 °C with a BTS-51800 Neware Battery Testing System (Shenzhen, China). A typical three-electrode test cell was used for cyclic voltammetry at room temperature. Cyclic voltammograms (CVs) were measured at different scan rates between 3.0 and 4.5 V using an electrochemical workstation (CHI660A).

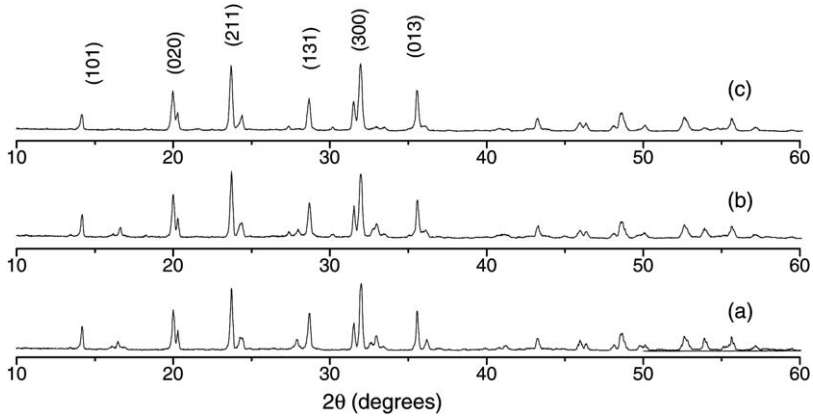

Fig. 2. XRD pattern of $NaV_{1-x}Cr_xPO_4F$ with different Cr doped amount. (a) $x = 0.00$, (b) $x = 0.04$ and (c) $x = 0.08$.

3. Results and discussion

The FT-IR spectrum of $NaV_{1-x}Cr_xPO_4F$ ($x = 0.00$, 0.04, 0.08) was shown in Fig. 1. It can be seen that a number of symmetric and anti-symmetric P–O stretching mode peaks appeared in the range of 1000–850 cm^{-1}, as well as P–O bending mode peaks below 700 cm^{-1} in Fig. 1. Especially, the band at 1050 cm^{-1}, assigned to the absorbed peak resulted by PO_4^{3-} anti-symmetric stretching [20], was observed to become narrow and its absorbance is increasing with the doped amount of Cr. Another, the bending vibration peak, at 580 cm^{-1} usually, is divided into several peaks, at 630, 559 cm^{-1}, etc. It is well known that the FT-IR spectrum of phosphates is mainly consisted of the inner-vibrated mode peaks of PO_4^{3-} group and some other groups. Thus, from the FT-IR spectrum of samples, it can be confirmed that this material is in phosphates type. Also, in the FT-IR spectrum of Cr doped materials, it was observed that the absorbance of peak increased comparing to the un-doped materials, and the band peak is moving to higher band numbers as the doped amount of Cr increase. So, it explains that the strength of V–O band increased with the doped Cr, and the crystal cell shrunk. So that it can be expected that the stability of materials will be enhanced and the cycle performance will be better with the introduction of Cr.

Fig. 2 is the XRD pattern of $NaV_{1-x}Cr_xPO_4F$ ($x = 0$–0.1) obtained by solid-state reaction, and its lattice parameters of crystal cell are shown in Table 1. From Fig. 2 and Table 1, it can indicate that the as-synthesized powder has the typical structure of a monoclinic type crystal with a space group of *C*2/*c*. The proposed structure is in good accordance with the structural analysis of the related compound, $Na_3Al_2(PO_4)_2F_2$ [21]. That is, the asymmetric unit of $NaVPO_4F$ consists of two PO_4 tetrahedra that share two corner-oxygen atoms with two different VO_4F_2 octahedra. The $V(1)O_4F_2$ and $V(2)O_4F_2$ octahedra are

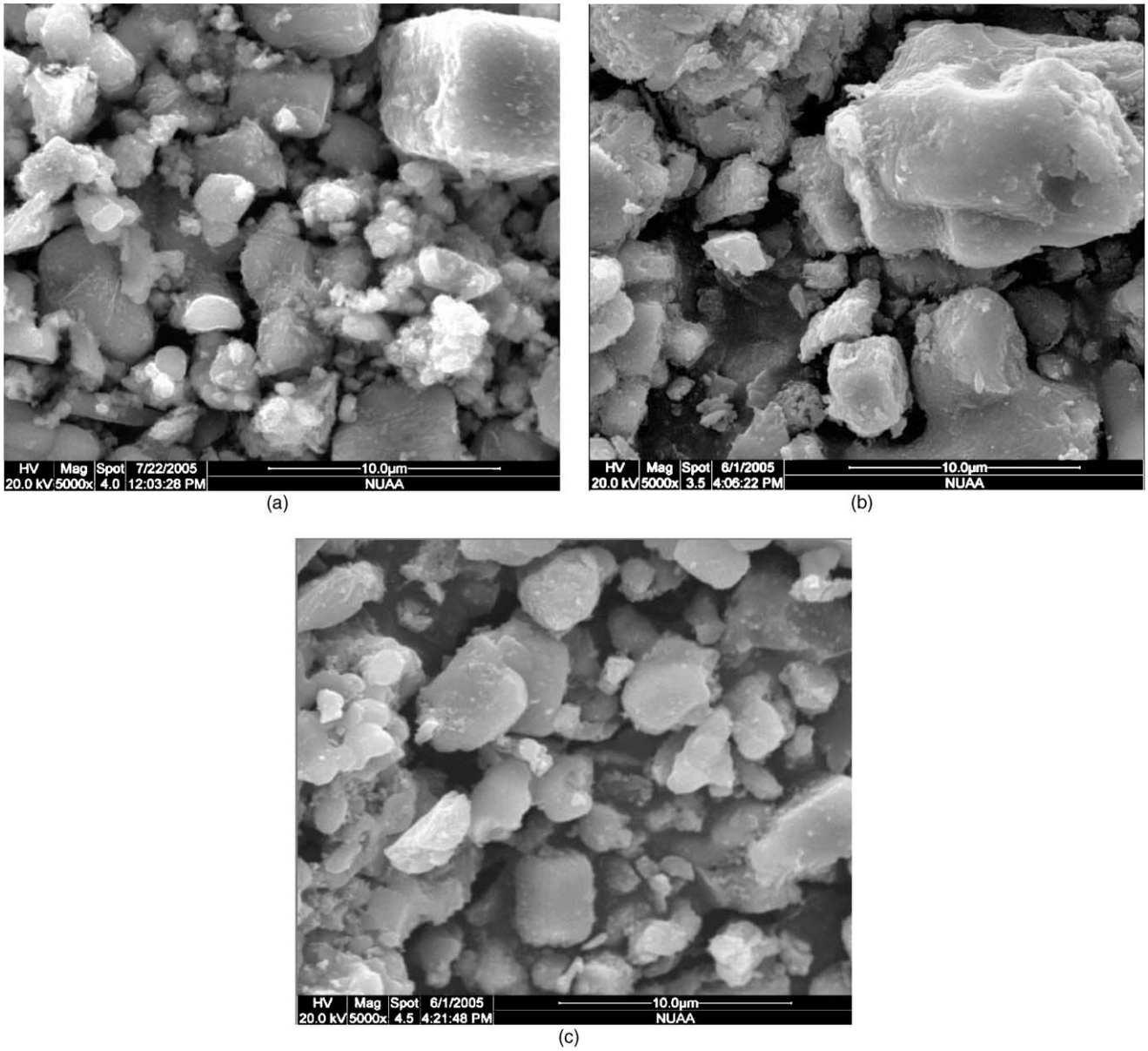

Fig. 3. SEM micrographs of samples with different Cr doped amount: (a) $NaVPO_4F$; (b) $NaV_{0.96}Cr_{0.04}PO_4F$; (c) $NaV_{0.92}Cr_{0.08}PO_4F$.

Table 1
The lattice parameters for samples

Sample	Cr (x)	a (nm)	b (nm)	c (nm)	α (°)	β (°)	γ (°)
$NaVPO_4F$	0.00	1.273	0.638	0.895	90.00	102.31	90.00
$NaV_{0.96}Cr_{0.04}PO_4F$	0.04	1.260	0.598	0.893	90.00	100.07	90.00
$NaV_{0.92}Cr_{0.08}PO_4F$	0.08	1.220	0.563	0.889	90.00	99.92	90.00

linked together via the F(1)-fluorine atom [22]. This distribution produces cavities in which the sodium ions are statistically distributed. To understand the influence of the Cr doping on the structure, Rietveld refinements were carried out for all compositions. Comparing with the un-doping Cr powder, it was observed from Fig. 2 that the diffraction peaks were shifted to a higher angle with the doping amount of Cr increasing, which indicates a gradual decrease in lattice parameters. The intensities of peaks are gradually increased by increasing Cr doping amount. The diffraction peaks were quite narrow, it indicates that the powder has a high crystallinity and no impurity diffraction peak was observed. The better crystalline properties the material is, the better structural stability during electrochemical cycle. The reason for the decrease of its structural parameter in Table 1 is primarily due to the difference in the ionic radius of Cr^{3+} (0.610 Å) and V^{3+} (0.640 Å). These results clearly confirmed that Cr substitution for V sites was successful and the single-phase solid solution was formed when the doped amount of Cr is increase to $x = 0.08$ (seen $NaV_{0.92}Cr_{0.08}PO_4F$).

Scanning electron microscopy (SEM) images of the $NaV_{1-x}Cr_xPO_4F$ ($x = 0$, 0.04, 0.08) powders are given in Fig. 3. It was observed that the average particle size is about 2–5 μm. and some cubic shape particles can be found in all of these samples. Maybe it is the macroscopical reflection of its monoclinic crystal structure. Also, in Fig. 3(c), it was observed that the size of particles is symmetrical. Comparing with the un-doped Cr sample, it can concluded that small amount of Cr-doping did not affect the powder morphology shown in Fig. 3(b) and (c).

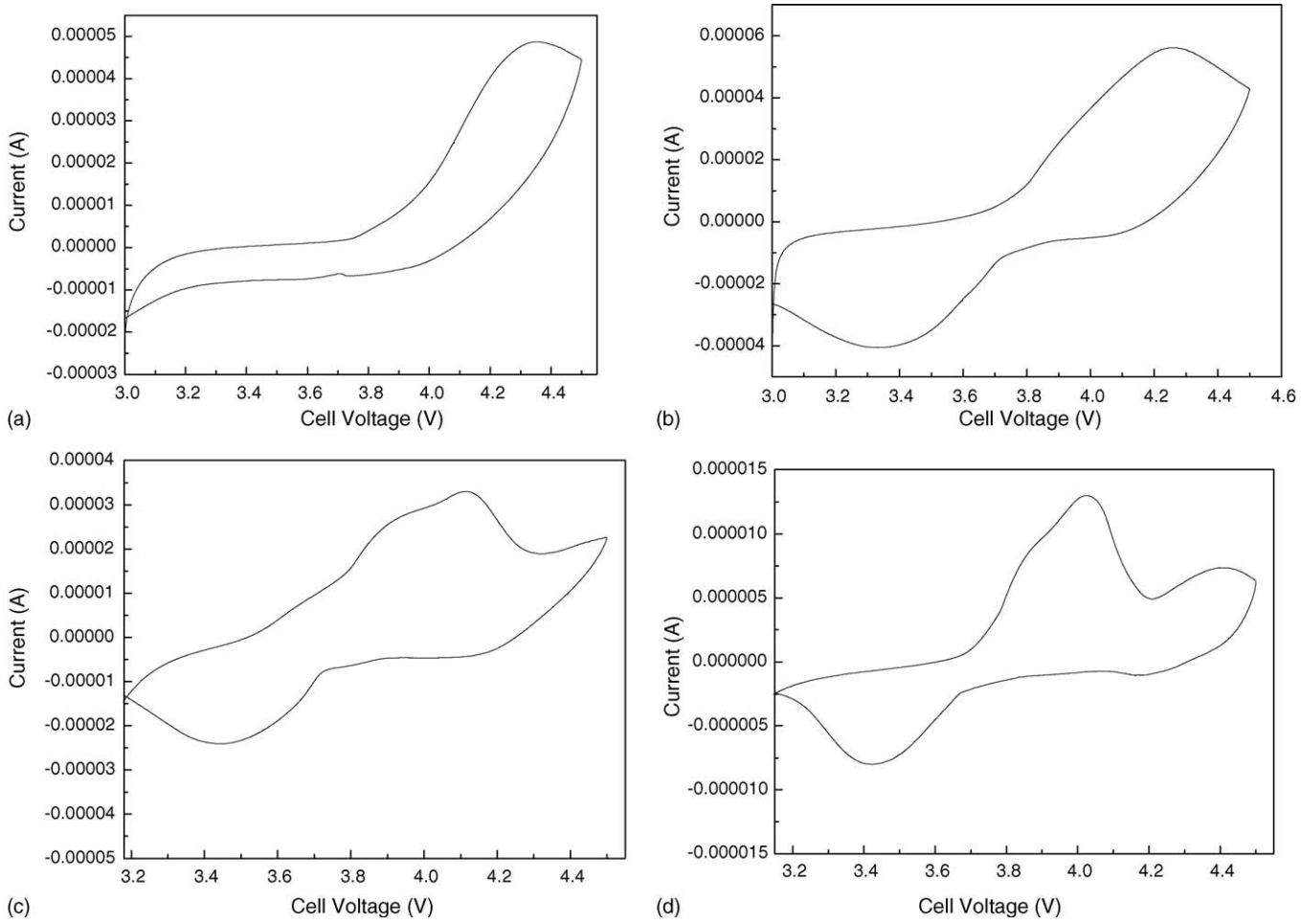

Fig. 4. Cyclic voltammograms of $NaVPO_4F$ electrode with different scan rate in the voltage range 3.0–4.5 V (scan rate: (a) 100 mV min^{-1}; (b) 50 mV min^{-1}; (c) 20 mV min^{-1}; (d) 5 mV min^{-1}).

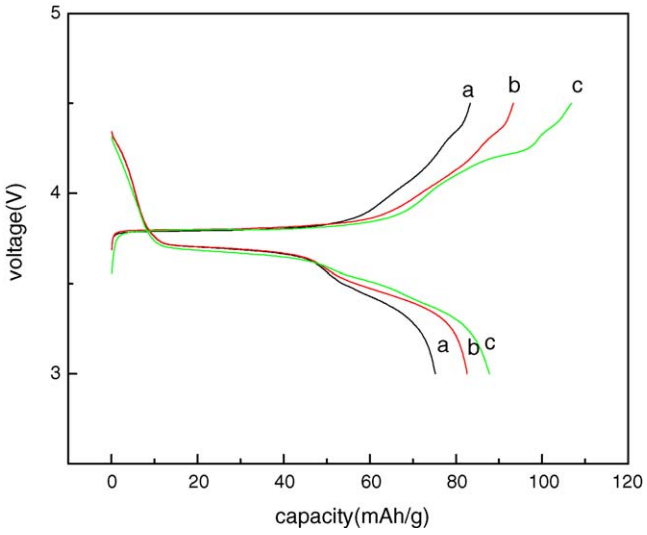

Fig. 5. The first charge and discharge capacity of $NaV_{1-x}Cr_xPO_4F$ electrodes. Data collected with a current density of 10 mA g^{-1} in the voltage range of 3.0–4.5 V: (a) $NaV_{0.92}Cr_{0.08}PO_4F$; (b) $NaV_{0.96}Cr_{0.04}PO_4F$; (c) $NaVPO_4F$.

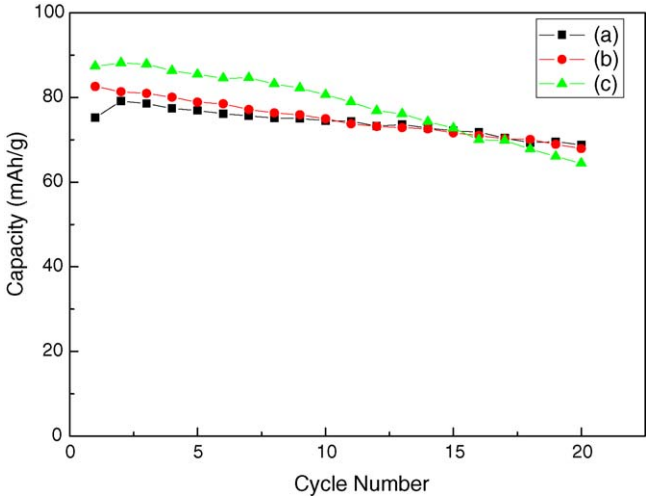

Fig. 6. Discharge capacity versus cycle numbers for Na/$NaV_{1-x}Cr_xPO_4F$ cells. Data collected with a current density of 10 mA g^{-1} in the voltage range of 3.0–4.5 V: (a) $NaV_{0.92}Cr_{0.08}PO_4F$; (b) $NaV_{0.96}Cr_{0.04}PO_4F$; (c) $NaVPO_4F$.

Fig. 4 shows cyclic voltammograms of $NaVPO_4F$ electrode with different scan rate in the voltage range 3.0–4.5 V. The cyclic voltammogram showed two couples of peaks in cathodic sweep and anodic sweep when scan rate are 20 and 5 mV min^{-1}. It agrees well with the two voltage plateaus of the charge/discharge curves for $NaVPO_4F$ in Fig. 5, which suggests that the intercalation and deintercalation of sodium-ion in the $NaVPO_4F$ were carried out in two steps. It can be seen obviously from Fig. 5 that two charge voltage plateaus are approximately 3.8 and 4.2 V, respectively, the equivalent discharge voltage plateaus are around 3.65 and 3.4 V, respectively. The cyclic voltammograms show two anodic peaks at around 4.3 and 4.0 V and cathodic peaks at 4.2 and 3.4 V at a scan rate of 5 mV min^{-1}. Thus, comparing the voltammograms curves in 20 and 5 mV min^{-1}, it can be found that the anodic and cathodic peaks potential shifted toward more positive direction. This suggests that the intercalation and deintercalation of sodium ions in the $NaVPO_4F$ were quasi-reversible. Another, it can also be observed in Fig. 4 that the redox peaks of $NaVPO_4F$ electrode are sharp and show well-defined splitting as the scanning rate increase, the potential separation between the two peaks increase with the scanning rate increase, it may be result from that the sodium ions cannot diffuse into the electrode surface when each fast cycle is completed.

Fig. 5 illustrates the cell voltage versus capacity curves for the first charge and discharge of $NaV_{1-x}Cr_xPO_4F$ electrodes ($x = 0$, 0.04, 0.08) between 3.0 and 4.5 V. Charge–discharge capacity and capacity retention ratio of the samples are tabulated in Table 2. The cathodes are first galvanostatically charged and subsequently discharged by application of a current density of 10 mA g^{-1} at 30 °C. The Cr-free $NaV_{1-x}Cr_xPO_4F$ had the initial discharge capacity of 87.7 mAh g^{-1}, showing a Coulombic efficiency of 82%. However, the cathode doped with 0.04 mol of Cr per formula unit delivered a decreased discharge capacity of 82.6 mAh g^{-1}, of which the efficiency corresponds to 88.5%. When $x = 0.08$ in $NaV_{1-x}Cr_xPO_4F$, the initial discharge capacity was only 75.2 mAh g^{-1} and the efficiency was up to 90.3%. Considering the Cr substitution amount, the reversible capacity is decreased by higher level Cr doping, but the efficiency is enhanced.

Fig. 6 show plots of the discharge capacity measured at room temperature as a function of the cycle number for $NaV_{1-x}Cr_xPO_4F$ electrodes ($x = 0$, 0.04, 0.08). The Cr-free sample showed the initial discharge capacity of 87.7 mAh g^{-1} and retained 73.5% of its original capacity at the 20th cycle (in Fig. 6(c)). As the Cr content increased up to $x = 0.08$, Na/$NaV_{1-x}Cr_xPO_4F$ cells exhibited some increased capacities and capacity retention, compared to those of $NaVPO_4F$. Especially, when $x = 0.08$, the capacity retention at the 20th was close to 91.4% of its initial discharge capacity. The

Table 2
Charge–discharge capacity and capacity retention ratio (%) of the samples

Cathode materials	The first charge capacity (mAh g^{-1})	The first discharge capacity (mAh g^{-1})	Capacity loss in the first cycle (mAh g^{-1})	Reversible efficiency in the first cycle (%)	The discharge capacity at the 20th (mAh g^{-1})	The capacity retention ratio at the 20th (%)
$NaV_{0.92}Cr_{0.08}PO_4F$	83.3	75.2	8.1	90.3	68.8	91.4
$NaV_{0.96}Cr_{0.04}PO_4F$	93.3	82.6	10.7	88.5	67.9	82.2
$NaVPO_4F$	106.9	87.7	19.2	82.0	64.5	73.5

results show that the as-prepared Cr-doped materials have a better cycle stability characterization than the un-doped one.

4. Conclusions

$NaV_{1-x}Cr_xPO_4F$ ($x = 0$–0.1) with the monoclinic structure were synthesized by the high temperature solid-state reaction and the effect of Cr doping on structure and electrochemical behaviors of $NaV_{1-x}Cr_xPO_4F$ were investigate. It has been confirmed that a small amount of Cr-doping did not affect their morphology, Cr substitution for V sites was successful and the single-phase solid solution was formed when the doped amount of Cr is increase to $x = 0.08$. A small amount of Cr doping gave rise to the electrochemical cycling properties of $NaV_{1-x}Cr_xPO_4F$. The results of cycling testing showed a preferable discharge capacity of about $80\,mAh\,g^{-1}$ and good capacity retention (91.4%). The cyclic voltammogram showed two couples of peaks in cathodic sweep and anodic sweep. It agrees well with the two voltage plateaus of the curve for $NaV_{1-x}Cr_xPO_4F$. Based on the available data, we believe that the $NaV_{1-x}Cr_xPO_4F$ doped with Cr will offer considerable promise as a viable cathode for sodium-ion batteries.

Acknowledgements

This work was financially supported by the National nature science foundation of China (grant no. 50472080), the Project of nature science foundation of Hunan Province under the grant (grant no. 04JJ3040, 05JJ20013), and the Project of nature science foundation of Jiangsu Province under the grant no. BK2003092.

References

[1] D.A. Stevens, J.R. Dahn, J. Electrochem. Soc. 147 (2000) 1271.
[2] P. Thomas, J. Ghanbaja, D. Billaud, Electrochim. Acta 45 (1999) 423.
[3] R. Alcantara, M. Jaraba, P. Lavela, J.L. Tirado, Chem. Mater. 14 (2002) 2847.
[4] D.A. Stevens, J.R. Dahn, J. Electrochem. Soc. 147 (2000) 4428.
[5] R. Alcantra, J.M.J. Metaeos, P. Lavela, J.L. Tirado, Electrochem. Commun. 3 (2001) 639.
[6] R. Alcantara, J.M. Jimenez Mateos, J.L. Tirado, J. Electrochem. Soc. 149 (2) (2002) A201.
[7] Y. Uebou, S. Okada, J. Yamaki, J. Power Sources 115 (2003) 119.
[8] M.M. Doeff, T.J. Richardson, J. Hollingsworth, C.-W. Yuan, M. Gozales, J. Power Sources 112 (2002) 294.
[9] W.U. Zhen-jun, Chen Zong-zhang, Tang Hong-Wei, Li Su-Fang, Battery Bimonthly 32 (2002) 45 (in Chinese).
[10] K. West, B. Zachau-christiansen, T. Jacobsen, Solid-State Ionics 28–30 (2) (1988) 1128.
[11] M.M. Doeff, Y. Ferry, Y. Ma, L. Ding, L.C. Dejonghe, J. Electrochem. Soc. 144 (1997) L20.
[12] M.M. Doeff, M.Y. Peng, Y. Ma, L.C. Dejonghe, J. Electrochem. Soc. 141 (1994) L145.
[13] S. Bach, M. Millet, J.P. Periera-Ramos, L. Sanchez, P. Lavela, J.L. Tirado, Electrochem. Solid-State Lett. 2 (11) (1999) 545.
[14] J. Barker, M.Y. Sadi, U.S. Patent 5,871,866, 1999.
[15] J. Barker, M.Y. Sadi, J. Swoyer, U.S. Patent 6,387,568, 2002.
[16] J. Barker, M.Y. Saidi, J.L. Swoyer, Electrochem. Solid-State Lett. 6 (2003) A1.
[17] J. Barker, M.Y. Saidi, J.L. Swoyer, J. Electrochem. Soc. 151 (10) (2004) A1670.
[18] S.-T. Myung, S. Komaba, N. Hirosaki, N. Kumagai, K. Arai, R. Kodama, Y. Terada, I. Nakai, J. Power Sources 119–121 (2003) 211.
[19] S.-T. Myung, S. Komaba, K. Hosoya, N. Hirosaki, Y. Miura, N. Kumagai, Chem. Mater. 17 (2005) 2427.
[20] Wen-Sheng Dong, Jonathan K. Bartley, Nian-Xue Song, G.J. Hutchings, Chem. Mater. 17 (2005) 2757.
[21] J.-M. Le Meins, M.-P. Crosnier-Lopez, A. Hemon-Ribaud, G. Courbion, J. Solid-State Chem. 148 (1999) 260.
[22] E. Alda, B. Bazan, J.L. Mesa, J.L. Pizarro, M.I. Arriortua, J. Solid-State Chem. 173 (2003) 101.